

# Measurement of identified charged hadron spectra in proton-proton collisions using the Inner Tracking System of the ALICE experiment at the LHC

Emanuele Biolcati

on behalf of the ALICE collaboration

*biolcati@to.infn.it*

**Abstract.** The measurement of the identified charged hadron  $p_t$  spectra using the ITS energy loss signal in the  $pp$  data at  $\sqrt{s} = 900$  GeV collected by the ALICE experiment at LHC will be discussed. It is performed using the Inner Tracking System (ITS) in stand-alone mode, both for track reconstruction and particle identification, allowing one to detect low momentum particles with  $p_t$  below 200 MeV/c. A second method using the tracks reconstructed by both the ITS and the Time Projection Chamber (TPC) has also been developed. The obtained results will be compared with the ones obtained from the TPC and from the Time Of Flight detector and used to extract the mean  $p_t$  value.

**Keywords:** ITS standalone, spectra

**PACS:** 25.75.Dw, 13.85.Ni

## INTRODUCTION

The measurement of identified charged hadron spectra in proton-proton collisions at  $\sqrt{s} = 900$  GeV has been performed by the ALICE experiment on the data collected in 2009 at LHC. The results provide basic insights into particle production processes and give the possibility to test and tune commonly used event generators at LHC energies. In addition, when repeated at higher energy, they will be the baseline for measurements in heavy-ion collisions.

The ALICE experiment features detectors that have multiple particle identification systems, including the Time Projection Chamber (TPC), the Inner Tracking System (ITS), a dedicated time-of-flight system (TOF). They allow ALICE to identify charged hadrons in the momentum range from 90 MeV/c up to 2.5 GeV/c. More details about the ALICE design can be found in [1]. Further information about the identified particle studies with this experiment can be found in [2].

The Inner Tracking System, close to the interaction point, is built of three sub-detectors, each of those contains two concentric Silicon layers. The innermost part is the pixel detector (SPD), the middle part is the drift detector (SSD) and the outermost one is the strip detector (SDD). The ITS provides high resolution tracking for the identification of secondary vertices of heavy flavour weak decays and improved momentum resolution at moderate  $p_t$ . The ITS is also used for stand-alone tracking to measure tracks at very low  $p_t$  not reaching the TPC.

## ITS ANALYSIS

The calculation of the identified charged hadron spectra in the ITS is based on the measurement of the particle energy loss in 4 (SSD and SDD) out of 6 Silicon layers. The ITS sub-systems have been aligned and commissioned using the cosmic data taken by the ALICE experiment in 2008, for more details see [3, 4, 5]. To achieve a precise charge calibration, the distribution of charge per unit path length has been measured and fine tuned for each module of the SDD and the SSD. In figures 1 and 2 it is possible to see that the peaks of the charge distributions are centered at the same value with a tolerance less than 5%.

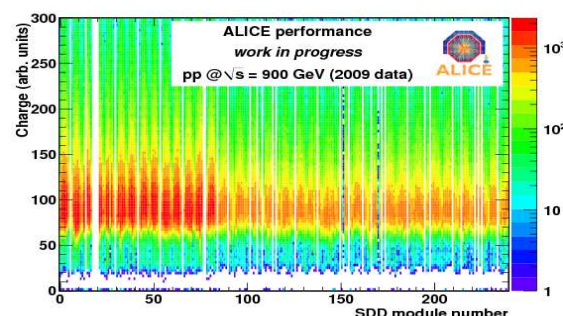


**FIGURE 1.** SDD charge distribution versus module number. More statistic for the inner layer (first 84 modules).

Two independent analyses have been performed using two different ITS track samples: the stand-alone ones, reconstructed using only information from the ITS (6 silicon layers) and the global ones, that use all the ALICE tracking detectors. In any case, only tracks with 3 or

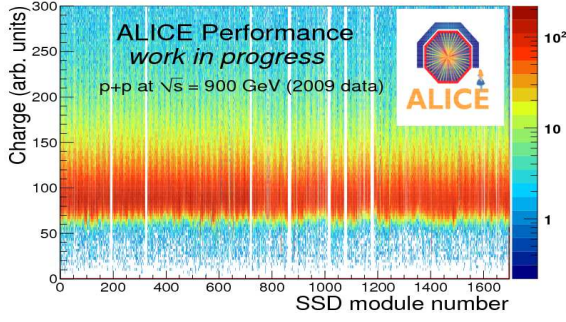


**FIGURE 2.** SSD charge distribution versus module number.

4 points localized in the SDD and SSD are used in the analysis. The charge deposit measured in each layer is normalised to the energy loss per  $300 \mu\text{m}$  (thickness of the ITS layers) of Silicon using the track local angles as reconstructed by the tracking algorithm. In the case of SDD clusters, a linear correction for the dependence of the reconstructed raw charge as a function on drift time due to the combined effect of charge diffusion and zero suppression is also applied [6]. For each track,  $dE/dx$  is calculated using a truncated mean: the average of the lowest two points in case 4 points are measured, or a weighted sum of the lowest (weight 1) and the second lowest point (weight 1/2) in case 3 points are measured. Figure 3 shows the energy loss signal so obtained in the ITS as function of the momentum for stand-alone tracks, compared to the parametrised response for pions, kaons and protons. This parametrisation is based on the Bethe-Bloch formula from [7], with an additional correction for the low momentum part.

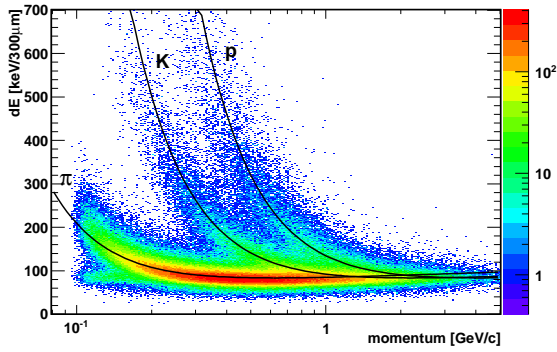


**FIGURE 3.** Energy loss signal versus momentum for the ITS stand-alone tracks. Three lines show the pion, kaon and proton signals expected by the Bethe-Bloch formula.

For each track fulfilling the track quality requirements, the rapidity is calculated using three different mass hypotheses: pion, kaon and proton. Tracks with  $|y| < 0.5$  are selected. For each hypothesis in  $p_t$  bins, a histogram

is filled with the difference between the logarithm of the measured energy loss signal in the ITS and expected value calculated using the variable

$$\xi = \log[dE/dx]_{\text{mean}} - \log[dE/dx]_{\text{calc}}.$$

This procedure gives a series of three histograms for each charged particle in all  $p_t$  bins. Figure 4 shows an example of these distributions for the kaon mass hypothesis.

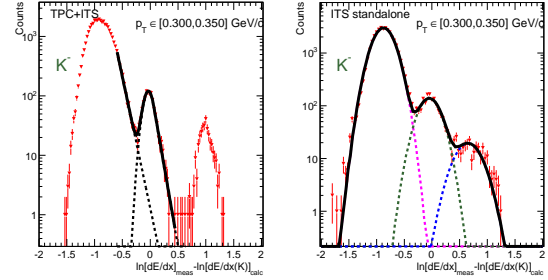


**FIGURE 4.** Distributions of the variable  $\xi$  in a  $p_t$  bin, in the kaon hypothesis mass, for the two ITS track samples. The fit curves are superimposed.

The area below the peak centered at zero is the raw yield of particles from the mass hypothesis in given  $p_t$  bin. The raw yield is determined by fitting the histograms with functions show in the figure 4: a sum of three Gaussians for the ITS stand-alone analysis and a sum of a Gaussian with an exponential tail and the tail of the peak at lower  $dE/dx$  for the TPC+ITS analysis. The raw yield is then corrected for the contamination from secondary particles and the overall efficiency. This has been calculated by using a Monte-Carlo simulation of the collisions and the detector in the same configuration of the data taking period. Figure 5 shows the overall efficiencies for the ITS stand-alone analysis for positive pions, kaons and protons. They take into account the geometric acceptance, the tracking efficiency, the dead channels and the K decays.

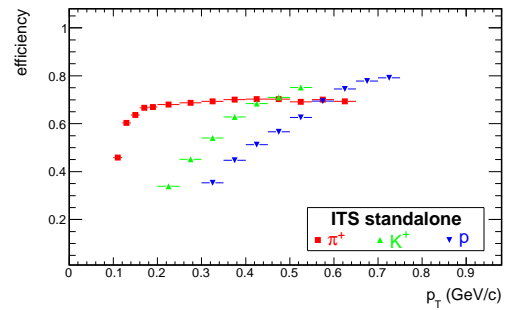


**FIGURE 5.** Overall efficiency of the ITS stand-alone versus  $p_t$ . Only positive pion, kaon and proton points plotted.

## RESULTS

After the correction, performed separately for each analysis, the yields have been normalized to the number of the inelastic collisions. The first important result is the coherence between the four independent analyses: ITS stand-alone, ITS+TPC, TPC and TOF. In figure 6 the matching of the points for the three positive species is observable. It is thus possible to cover the whole transverse momentum range from 90 MeV/c to 2.5 GeV/c.

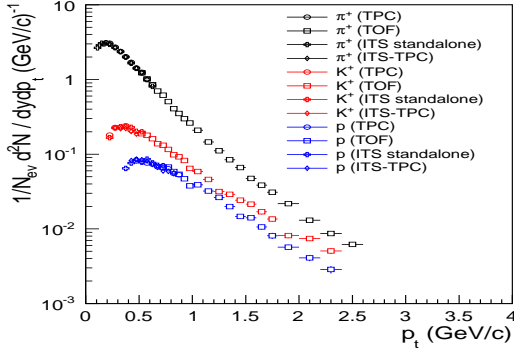


**FIGURE 6.** Identified particle spectra obtained by the four independent analyses using ITS, TPC and TOF (positive only).

The spectra have been combined weighting for the uncorrelated systematic errors and fitted using the Lévy function [8]:

$$\frac{d^2N}{dp_t dy} = p_t \frac{dN}{dy} \frac{(n-1)(n-2)}{nC(nC+m(n-2))} \left(1 + \frac{m_t - m_0}{nC}\right)^{-n}.$$

In figure 7 the fit result for the positive particles is shown.

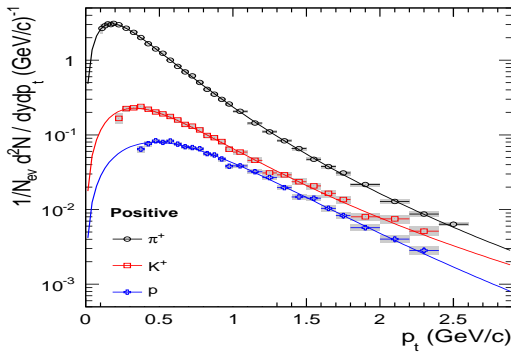


**FIGURE 7.** Transverse momentum spectra of positive hadrons from pp collisions at  $\sqrt{s} = 900$  GeV. Grey band: total  $p_t$ -dependent error (systematic plus statistical); normalization systematic error not plotted.

The mean transverse momentum, extracted from the fit, has been compared with the results obtained in  $pp$  collisions at  $\sqrt{s} = 200$  GeV and in  $\bar{p}p$  reactions

at  $\sqrt{s} = 900$  GeV. The mean  $p_t$  rises very little with increasing  $\sqrt{s}$  despite the fact that the spectral shape clearly shows an increasing contribution from hard processes. It was already observed that at RHIC energies the increase  $\langle p_t \rangle$ , compared to studies at  $\sqrt{s} = 25$  GeV, is small (figure 8).

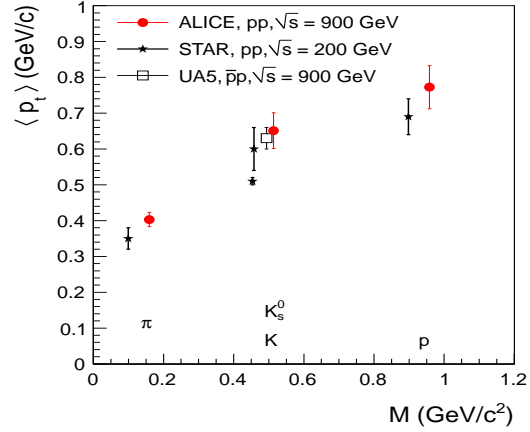


**FIGURE 8.** Mean  $p_t$  versus the mass of the emitted particle obtained in  $pp$  collisions at  $\sqrt{s} = 200$  GeV and at 900 GeV and also in  $\bar{p}p$  at  $\sqrt{s} = 900$  GeV.

## CONCLUSIONS

This measurement is an important confirmation about the good operation of the central detectors of the ALICE experiment for  $pp$  collisions. As a matter of fact, the analyses performed using different detectors and different approaches give a coherent result, allowing to cover a large transverse momentum range.

The first identified hadron  $p_t$  spectra from proton-proton collisions at LHC have been analyzed. In this way, the whole analysis framework has been tuned in order to repeat the study for  $pp$  data at higher energies.

## REFERENCES

1. K. Aamodt *et al.* [ALICE Collaboration], JINST **3** (2008) S08002.
2. P. Christakoglou, these proceedings
3. K. Aamodt *et al.* [ALICE Collaboration], JINST **5** (2010) P03003
4. B. Alessandro *et al.*, JINST **5** (2010) P04004
5. P. Christakoglou [ALICE Collaboration], PoS E PS-HEP2009 (2009) 124
6. B. Alessandro *et al.*, JINST **5**, (2010) P02008
7. B. Alver *et al.* [PHOBOS Collaboration], Phys. Rev. C **75** (2007) 054913
8. B. I. Abelev *et al.* [STAR Collaboration], Phys. Rev. C **79**, 034909 (2009).